A novel design and manufacturing method for compliant bistable structure with dissipated energy feature

Pan, Diankun; Wu, Zhangming; Dai, Fuhong; Tolou, Nima

DOI
10.1016/j.matdes.2020.109081

Publication date
2020

Document Version
Final published version

Published in
Materials and Design

Citation (APA)
Pan, D., Wu, Z., Dai, F., & Tolou, N. (2020). A novel design and manufacturing method for compliant bistable structure with dissipated energy feature. *Materials and Design*, *196*, Article 109081. https://doi.org/10.1016/j.matdes.2020.109081

Materials and Design 196 (2020) 109081

Contents lists available at ScienceDirect

Materials and Design

journal homepage: www.elsevier.com/locate/matdes

A novel design and manufacturing method for compliant bistable structure with dissipated energy feature

Diankun Pan [a], Zhangming Wu [a,*], Fuhong Dai [b,*], Nima Tolou [c]

[a] Key Laboratory of Impact and Safety Engineering, Ministry of Education of China, Ningbo University, Ningbo 315211, China
[b] National Key Laboratory of Science and Technology on Advanced Composites in Special Environment, Harbin Institute of Technology, Harbin 150001, China
[c] Faculty of Mechanical, Maritime and Materials Engineering, Department of Precision and Microsystems Engineering, Delft University of Technology, Mekelweg 2, 2628 CD Delft, the Netherlands

HIGHLIGHTS

- A novel bistable structure is designed and fabricated successfully by the pulsed laser machining technique.
- The bistable structure can be mounted under the cantilever boundary and exhibits strong hysteresis and feature of energy dissipation.
- The bistability of the proposed structure can be adjusted by processing parameters and geometry parameters.

GRAPHICAL ABSTRACT

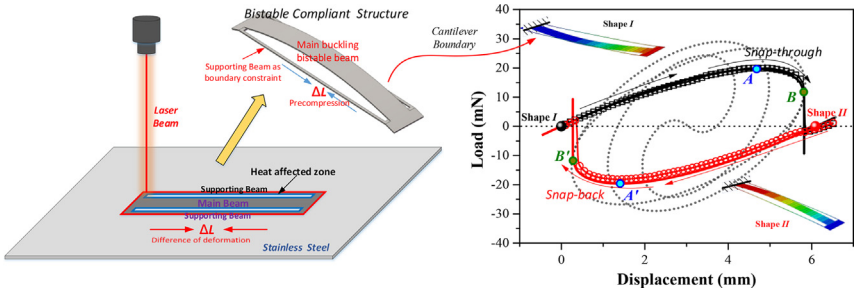

ARTICLE INFO

Article history:
Received 9 June 2020
Received in revised form 12 August 2020
Accepted 20 August 2020
Available online 22 August 2020

Keywords:
Bistable structure
Snap-through
Cantilever
Pulsed laser
Hysteresis

ABSTRACT

In this paper, a novel design concept and manufacturing method for the compliant bistable structure is proposed. The pulsed laser technique is utilized as the manufacturing method for both the fabrication and the introduction of desired pre-stresses, simultaneously. Based on this concept, a novel bistable structure consisted of one pre-compressed main beam, and a pair of supporting beams is designed and fabricated. The deformation difference between the main beam and the supporting beams induced by laser heating residual stress make the main beam to buckle under the constraints of two supporting beams and possess a bistable feature. The bistable structures can be implemented into other devices in the form of cantilevers thanks to the internal integration of the buckled beam and the boundary conditions. The characteristics of this new bistable structure, including its stable shape and snap-through response, are investigated both experimentally and numerically. During the snap forth and back process with the snapping load of 19 mN and the required energy of 77 mN·mm, an impressive energy dissipation with a loss factor value of 0.3 exists. Finally, a parametric study was carried out to find the critical performance parameters.

1. Introduction

As one typical type of compliant structure, bistable curved beams have many energy-related and motion-related applications from macro-word to the microelectromechanical systems (MEMS), such as energy harvesters, sensors, and actuators, due to their attractive mechanical behaviors: negative stiffness and two equilibrium stable positions [1].

There are two typical categories of bistable beams: pre-shaped bistable beams and pre-compressed bistable beams [2]. The pre-shaped bistable beams are designed with a certain shape without inducing any residual stresses. Qiu et al. [3] presented a bistable structure comprised of a pair of cosine-shaped parallel beams with a central connection, and an analytical solution of the lateral force and the center

* Corresponding authors.
E-mail addresses: wuzhangming@nbu.edu.cn (Z. Wu), daifh@hit.edu.cn (F. Dai).

https://doi.org/10.1016/j.matdes.2020.109081

deflection during the snap-through process was found to support its design. Hao et al. [4] made a comprehensive static analysis for the bistable mechanism composed of two inclined beams connected in the middle. Moreover, the pre-shaped bistable beam is often employed as the unit cell of the metamaterials or metastructure. Ha et al. [5] designed a lattice comprised of multiple tetra-beam-plate unit cells, and it exhibited an energy absorption feature when the unit cell occurs snap-through behavior. Valencia et al. [6] presented a multistable cellular material with the ability to dissipate energy through cell-level elastic instabilities. Tan et al. [7] proposed a type of metamaterial with a cylindrical shape which is composed of bistable curved beams. The pre-shaped bistable beams have a simple structure form and can be efficiently fabricated by the etching technique for MEMS [3], and it is easy for the metamaterials to manufacture by the 3D-printed technique. However, the force-displacement response of the pre-shaped bistable beam is asymmetric, which limits its applications, such as energy harvester.

The pre-compressed bistable beams with either clamped-clamped or pinned-pinned boundary conditions are typically a buckled beam that has been prescribed a compression displacement or a compression force along the axial direction. The pre-compressed beam is one of the most commonly used bistable structures, and its two stable equilibrium positions are the first two buckling mode shapes. The pre-compressed bistable beam is potentially applied in energy harvesters and actuators due to its advantages of symmetrical output load and adjustable out-of-plane motion [8]. Most of the investigation about the pre-compressed bistable beam focus on its snap-through properties. Camescasse et al. [9,10] presented the modeling for the snap-through response of the pinned-pinned pre-compressed beam and validated by experiments. Cleary and Su [11] established a model to analyze the snap-through behavior of a clamped-clamped pre-compressed beam actuated by a moment input. Nistor et al. [12] studied the relationship between the Euler buckling configurations and the load-displacement curve of the pinned-pinned pre-compressed beam. Gao et al. [13] proposed a novel method to design the clamped-clamped pre-compressed beam with desired snap-through properties. Taking the clamped-clamped pre-compressed beams as elements, Zhang et al. [14] proposed a type of multistable metastructure exhibiting both level and tilted stable configurations.

For the macro-world, the pre-compression is easy to perform by boundary conditions or external load, but the application of boundary conditions and external loading is not easy due to the limitation of space. Therefore, the pre-compression is better to be accomplished during the machining process for the micro-scale. At present, there are very few methods that are able to fabricate the pre-compressed bistable beam on the micro-scale. One typical method is making use of the thermal oxidation process to induce residual compressive stress after etching [15,16]. However, in this method, the depth of oxidation is difficult to be controlled. Therefore, it is hard to achieve or control the residual stress to obtain the pre-compression in such micromachining processes. Moreover, the etching machining process is generally expensive and time-consuming. It is necessary to develop alternative solutions to fabricate the pre-compressed bistable beam.

The pulsed laser technology is widely used in engineering, such as cutting [17], drilling [18], milling [19], and additive manufacturing [20–22], and is studied in terms of theory and simulation. Due to high-accuracy and high-speed, the pulsed lasers including nanosecond and femtosecond are widely employed as the ablation methods in the fabrication of MEMS components [23,24]. Laser machining is naturally a thermal process. When the laser beam with high energy density is focused on the workpiece, the temperature gradient structure leads to residual stresses developed in the region of the machining section. High levels of residual stresses may be achieved with well-selected machining conditions and material properties [25]. It is well known that a beam heated from the original stress-free configuration with constrained edges will have axial compressive stress developed inside it. Thus, the laser-machined beams with constraints will buckle when the residual stresses induced by laser heating reach a critical value.

In this paper, we introduce a new alternative method for obtaining a pre-compressed bistable structure utilizing the pulsed laser machining process. One typical structure with one wide main beam and a pair of narrow supporting beams is designed and fabricated by a pulsed laser in a single processing step. After the machining process, a pre-compression given by the deformation difference between the main beam and supporting beams will apply to the main beam and enable a bistable feature. In doing so, the supported boundary conditions can be achieved internally inside this integrated structural form, which enables us to design a cantilever-type bistable structure. The cantilever boundary enables the structure to obtain large out-of-plane displacement during the transition of stable states. The snapping load can be also lowered under this boundary. This new bistable structure takes advantage of the pulsed laser machining as the fabrication method and pre-stressing method simultaneously and integration of pre-compressed beam and constraints, therefore, it allows the manufacturing of small-size bistable structures. Moreover, the pulsed laser machining is of a quick and efficient manufacturing method, and its abundant process parameters provide extensive adjusting space to achieve the desired bistability features.

To fabricate this pre-compressed bistable structure with optimal bistability features, it is worthwhile to understand its snap-through behavior and the effects of key parameters that affect its behavior. The characteristics of the performance of this new bistable structure are verified both experimentally and numerically after the fabrication concept is validated. A parametric study is also carried out to determine the critical parameters that can affect the performance of this new bistable structure including stable shapes and snapping properties.

2. Conceptual design

This new concept is derived from the pre-compressed elastic pinned-pinned beam, as shown in Fig. 1(a). An initially straight beam of length l_0 along the x-axis is compressed by a certain distance Δl along its length to a new end length of l, resulting in the relationship of $l_0 = l + \Delta l$. The pre-compression of Δl gives rise the beam to buckle into one of the shapes shown in either red solid line or red dot-dash line. In doing so, the pre-compressed pinned-pinned beam becomes bistable. When an axial compression force is increased greater than a critical value, the beam will buckle into its first bucking mode. The first buckling

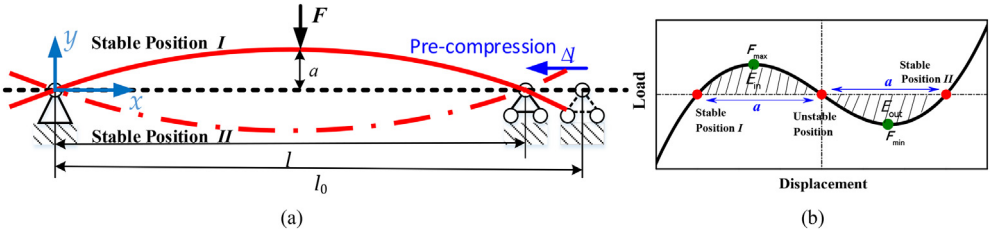

Fig. 1. (a) A pre-compressed elastic pinned-pinned beam; (b) Force-displacement curves of snap-through behavior.

mode for an elastic buckling beam is defined by the Euler-Bernoulli theory. For a pinned-pinned beam, it is given by,

$$y = a\sin\left(\frac{\pi x}{l}\right) \tag{1}$$

where a is the bending displacement in the central point of the beam when the pre-compression is Δl. The axial pre-compression Δl of the beam is approximatively given by [26],

$$\Delta l = \int_0^l \frac{1}{2}\left(\frac{\partial y}{\partial x}\right)^2 \mathrm{d}x \tag{2}$$

Thus, the stable shape of the pinned-pinned bistable buckling beam can be adjusted by this pre-compression.

When the buckling beam is loaded laterally shown in Fig. 1(a), the buckling beam may jump from one stable state to the other, which is referred to as a snap-through behavior. The typical relationship between lateral force and midpoint displacement of snap-through behavior is described in Fig. 1(b). There are three zero-force-crossings (marked by the red filled circles in Fig. 1(b) where the applied force is equal to zero), two of which represent two stable equilibrium positions. One of the most important features of the pre-compressed beam is that its force-displacement curve is symmetrical to the displacement axis, namely, the absolute value of minimum load F_{min} is equal to maximum load F_{max} and the distance between two stable positions and unstable position is the same. Furthermore, the input energy E_{in} is equal to the output energy E_{out}.

The pre-compression can be realized by applying either an axial force or the displacements supplied by the extra parts in macroscale size. However, it is difficult to realize the pre-compression when the dimension becomes very small, such as mesoscale and microscale. We design a new bistable prototype illustrated in Fig. 2(a). The design in the plane is a rectangle with two rectangular slits which are symmetric about the longitudinal axis. These two slits separate the prototype into one middle main beam with a wider width (W_1) and a pair of supporting beams with a much smaller width (W_2), and the remainder of the prototype connects the main beam with supporting beams. The length of the whole design is L_1, and the length of the slit, namely length of the main beam and the supporting beams is L. If supporting beams become shorter than the main beam, the change of the length ΔL acts as the pre-compression on the main beam, which will induce the occurrence of buckling. Here, the heating method is applied using a single pulsed laser-machining method. The heating load acts on the supporting beams and thus making the supporting beam shrink more than the main beam. The length of supporting beams is shorter than that of the main beam after the heating process, and as a result, the different deformation will function as the axial compressive displacement ΔL applying to the main beam.

The difference ΔL of heating deformation between the main beam and supporting beams can be approximatively expressed as:

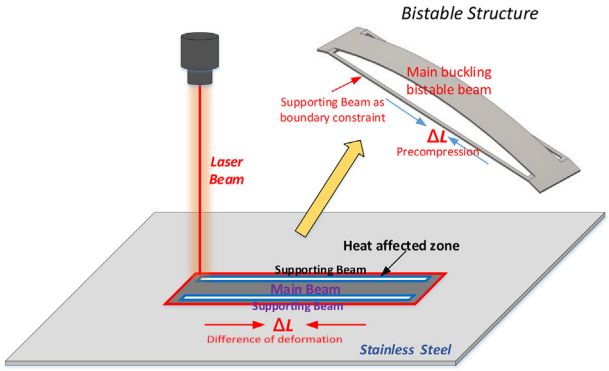

Fig. 3. The schematic diagram of the laser machining process for the prototype.

$$\Delta L = \alpha L \Delta T \tag{3}$$

where α is the linear thermal expansion of coefficient, L is the initial length of supporting beam and the main beam, and ΔT is the equivalent temperature gradient between the main beam and supporting beams due to the heating. The supporting beam influenced by this equivalent temperature gradient will shrink and its shrinkage acts as a pre-compression to the main beam. Fig. 2(b) is given by Eqs. (1) to (3), which shows the buckling configurations of the main beam with different equivalent temperature gradients. With the increase of temperature gradient, the main beam will be compressed more seriously.

The laser machining process involves the heating of the substrate material and can be utilized as the above heating method. The temperature at the cutting surface in contact with the laser beam reaches the melting temperature. As the laser beam passed the melted surface, the surface cools down due to radial heat conduction and convection, which results in a rapid variation of temperature in the region close to the cutting surface [27]. Due to this high-temperature gradients and rapid cooling rates in this region, a residual stress field is generated in this small region next to the cutting edges, namely, the heat-affected zone. In this paper, we exploit the residual stresses induced by laser heat to pre-stress the beams and form the aforementioned bistable prototype. As shown in Fig. 3, the prototype is cut by a pulsed laser from a monolithic substrate in a single processing step. The prototype comprises three closed polylines that are cut by a laser beam separately. The two slits emerge when the two blue polylines are finished, and the prototype still resides in the substrate plate at this moment. Then, the prototype will separate from the substrate plate when the outer red polyline is cut through.

The residual stress in the heat-affected zone has a much stronger influence on supporting beams than the main beam because two heat-affected zones of supporting beams are closer to each other than that of the main beam. Although the same laser machining conditions are employed in the single process step, the difference of deformation

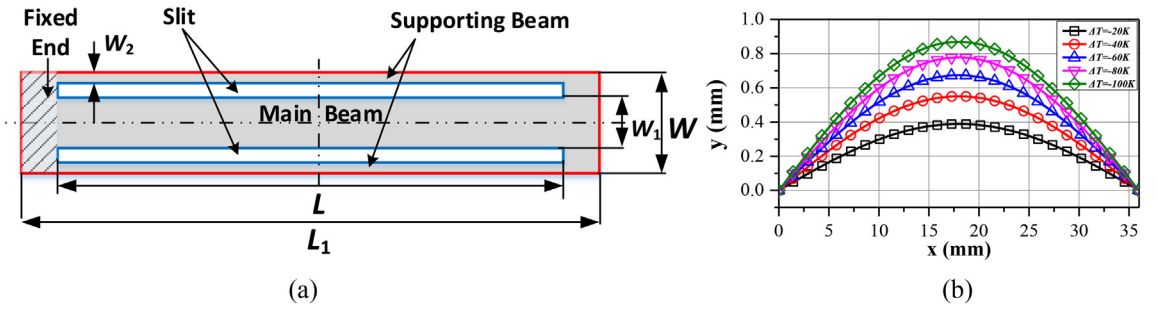

Fig. 2. (a) The geometry of the prototype; (b) Buckling configurations under different equivalent temperature gradients ($L = 36$ mm, $A = 0.36$ mm^2, $E = 187.5$GPa).

between the main beam and supporting beams arises because of their different widths. After the laser machining process, the difference of deformation can function as the axial compression ΔL applying to the main beam. The main beam will exhibit the bistability feature that is analogous to a pre-compressed buckled beam supported by two tension strings, as illustrated in Fig. 3.

Before the fabrication of this proposed bistable structure, it is worthwhile to further understand its forming condition, and then obtain the factors which determine its bistability. It is generally known that the load P_{crit} that causes the buckling of the main beam is

$$P_{crit} = \pi^2 EI/L^2 \tag{4}$$

where EI is the rigidity of the main beam. We postulate a tensile stress σ_n induced by the laser machining process in the supporting beam. This stress gives rise to compressive load P in the main beam, which is represented by

$$P = 2\sigma_n W_2 t \tag{5}$$

where t is the thickness and W_2 is the width of the supporting beam. If this applied compressive load P increased to become greater than P_{crit}, the main beam will buckle. The stress σ_n that can lead to buckling should satisfy

$$\sigma_n \geq \frac{\pi^2 E W_1 t^2}{24 W_2 L^2} \tag{6}$$

From Eq. (6), it is found that the feasibility of this bistable structure depending on two types of parameters, which are laser processing parameters depending on stress σ_n and geometry parameters (L, W_1, W_2, t). Due to the quadratic relationship, the length L and thickness t are concerned primarily. We used Eq. (6) with the material properties and the geometry parameters in Table 1 to generate a "map" of stress σ_n versus length L and thickness t that gives rise to buckling, as shown in Fig. 4. The shorter and thicker beam needs higher stress σ_n to form the buckling mechanism. The level of stress σ_n depends on the laser processing process and material properties, so it is carried out under certain restrictions. Therefore, the thin stainless steel with a high thermal expansion coefficient is selected to verify the proposed design.

The method does not confine to the prototype in Fig. 2(a). For this method, the deformation difference between beams introduced by the pulsed laser, namely pre-compression is the key, which is realized by the design of internal structural forms and integrated boundary conditions or constraints. The deformation difference can be caused by different geometry parameters or different laser processing parameters, which expand the design flexibility of bistable or multistable properties. In this work, the simple case shown in Fig. 2(a) is taken as an example to illustrate the feasibility of this method and the basic features of the proposed bistable structure. However, the deformation of beams depends on the level of residual stress induced by laser. Understanding the formation mechanism of this residual stress is an important issue to study with more efforts in the future. So, the formation of residual stress is not concerned deeply and the final status after fabrication is a priority to this work.

3. Experiments

3.1. Fabrication

To verify the proposed conceptual design, the samples were fabricated from a stainless steel plate using a Spectra-Physics Talon 355–15 diode-pumped solid-state (DPSS) UV laser system with a wavelength of 355 nm and the maximum power of 15 W at 50 kHz. The workpiece is placed on a ceramic substrate which is fixed by the vacuum extractor from beneath and moved on a high-precision three-axis motion stage controlled by a custom CAD-CAM (Computer-Aided Design, Computer-Aided Manufacturing) software. The optical steering is achieved by a Galvo heat from Rhothor with a scan range of 46 × 46 mm and a focal length of 100 mm. An overview of the setup is illustrated in Fig. 5(a). For improving the cutting quality while the focal point is moving inward to the material, re-focus after a certain depth is necessary to avoid out-of-focus. The thickness of the stainless steel plate is 98 μm, so three re-focus levels are adopted, and the step of the level is 50 μm. Additionally, four redundant lines with a gap of 10 μm are used for each polyline to guide the laser beam move into the workpiece, as shown in Fig. 5(b).

The laser parameters are selected carefully as follows: the pulse repetition rate is 50 kHz, the average power is 12.4 W and the scan speed is 20 mm/s. Table 1 lists the materials parameters and geometry parameters of the prototype. After the laser machining process without any extra operations, the prototype has two stable shapes when it is taken from the substrate, as shown in Fig. 5(c). As expected, the main beam is buckled due to the axial compression constraint of two slender supporting beams.

3.2. Measurements

The snap-through properties of the bistable pre-compressed beam with lateral load have been investigated extensively [9,10,12]. Benefiting from the integration of constraint conditions and pre-compressed beam, the proposed bistable structure can be connected with other components in the form of a cantilever configuration. Therefore, the study of the snap-through behavior of the prototype under cantilever boundary condition is our research emphasis in this paper.

A test set-up was established to measure the snap-through properties, which consist of a load cell (FUTEK LSB200), a movable stage, and a laser displacement sensor, as shown in Fig. 6(a). The movable stage can be actuated by a motor to move forth and back along the linear guideway, and the moving distance is controlled by the program and is measured by the laser displacement sensor. In the experiments, one end of the sample was clamped on a frame, and the other end was restricted to the load cell by two nuts, but it still can rotate, as shown in the magnification box of Fig. 6(a). The boundary condition of the free end is similar to a simply supported condition. The measurement of inherent load-displacement response during snap-through behavior is the purpose of this testing, so it needs to exclude the influence of possible squeezing. The load cell which was mounted on the movable stage can move forward with a given displacement firstly and then move back to the starting point, so the snap-through and snap-back responses can be triggered in one testing. The moving speed of the stage is slow in order to compare with the static results predicted by the finite element model. The starting measurement point of the load was adjusted to be

Table 1
Overview of material and geometrical parameters.

Material	Elastic Modulus E		Poisson's Ratio ν		The coefficient of thermal expansion α	
	187.5 GPa		0.28		14.4×10^{-6}/°C	
Geometry	Total length L_1	Total width W	Thickness t	Length L	Width W_1	Width W_2
	40 mm	7 mm	98 μm	36 mm	3.6 mm	0.2 mm

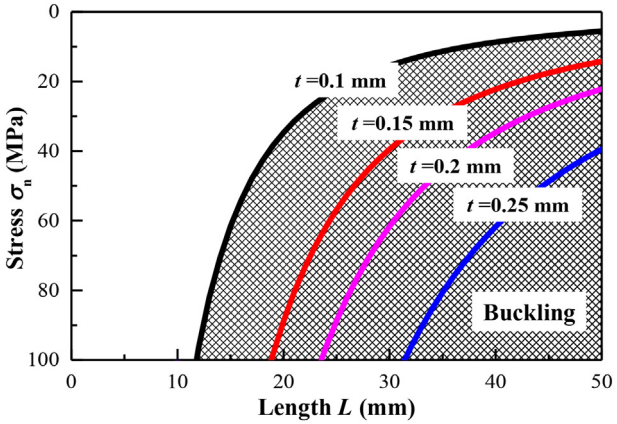

Fig. 4. Stress σ_n of the supporting beam that causes buckling.

zero which means the sample is in one stable state. The vertically applied load and the displacement were controlled and recorded at the same time by a Labview program. In this way doing so, the load-displacement curves during snap-through and snap-back processes are obtained within one testing.

Besides the snap-through properties, the stable shapes of the main buckling beam reflecting the level of pre-compression induced by laser heat are also important for the study of this bistable mechanism. The shapes can be represented by the out-of-plane displacement of its central line. Here, we measured the out-of-plane displacement of two stable shapes for each sample with the setup as shown in Fig. 6(b). The same measurement platform as the load-displacement testing setup was employed and the load cell was replaced by a movable plane. The sample was placed on this movable flat plane and a laser displacement sensor installed vertically above the sample is used to measure the displacement of the main beam when the sample is moving with the plane. The movable plane was considered as the zero reference and the out-of-plane displacement of the central line of the main beam was obtained, which is used to represent the stable shape and to compare with the results given by the finite element model.

4. Finite element analysis

A finite element analysis (FEA) by the commercial software ABAQUS is employed to verify the basic concept of this bistable structure proposed in this paper. Due to the small thickness, the shell element (S4R, 4-node doubly cured shell) is utilized, and the switch of 'Nlgeom' (geometrically nonlinear algorithms) is on during the entire analysis. The convergence study and efficiency analysis are carried out to obtain a mesh size of 0.5 mm. The final status of this bistable structure after fabrication is concerned primarily, so the residual stress development and transient physical effects during the laser machining process are not considered in this simulation. The material properties are listed in Table 1.

The stable shape after fabrication is obtained by two 'Static, General' steps. To simulate the pre-compression caused by the deformation difference between the main beam and supporting beam, a negative temperature gradient of ΔT is applied to two supporting beams. The center of the main beam is fixed as the boundary condition and a small out-of-plane displacement as a disturbance is applied to the four corners of the prototype to obtain the convergence in the first step. In the second step, the disturbance is removed and then the stable shape is found. The two stable shapes predicted by FEA are shown in Fig. 7(a), and the out-of-plane displacement of the central line can be extracted to compare with experimental results.

For the simulation of snap-through behavior under cantilever boundary, one end of the prototype is clamped and the other end is free, as shown in Fig. 2(a). The first two 'Static, General' steps are utilized to obtain stable shapes as before, as illustrated in Fig. 7(b). ABAQUS offers two static methods, namely 'Riks' and 'Stabilize', both are capable of studying this behavior. The 'Riks' method can trace the nonlinear equilibrium path even in the case of reversal loading, and the 'Stabilize' method can provide the load-displacement curves reflecting the actual situation like the experiments. These two methods are implemented for tracing this nonlinear snap-through behavior in this paper. For the 'Riks' method, another 'Static, Riks' step with a load applying to free end is required to simulate this snap-through behavior. However, two more 'Static, General' steps are needed for the 'Stabilize' method. In the third step, a displacement load at the free end is applied

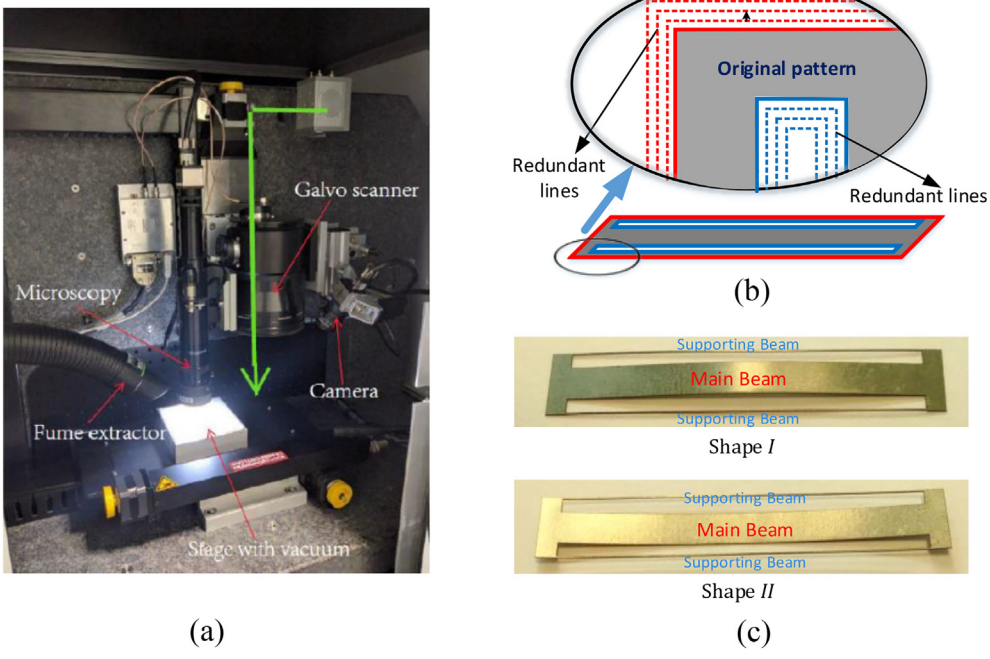

Fig. 5. (a) Laser beam setup; (b) Schematic representation of redundant lines and separating gaps used in laser machining; (c) Two stable shapes of the laser-machined bistable structure.

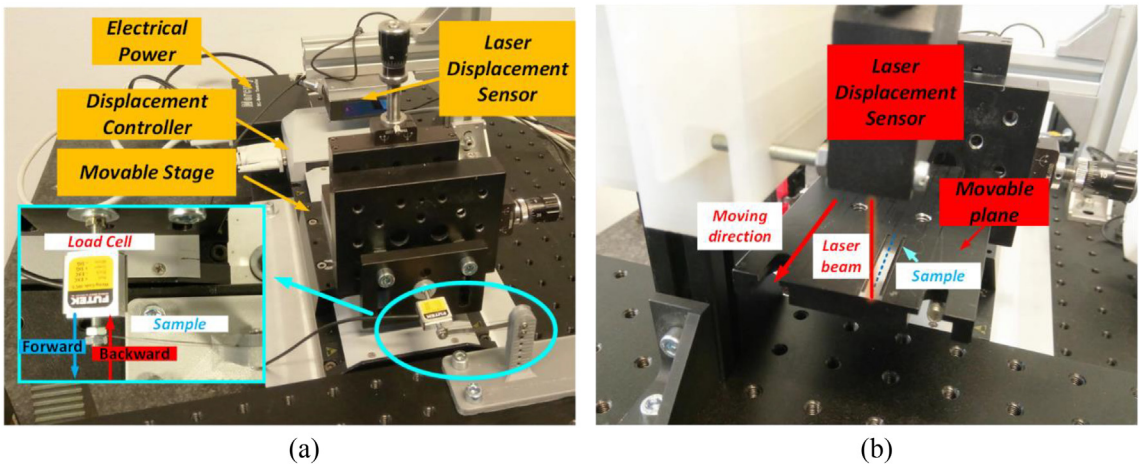

Fig. 6. (a) Test set-up for load-displacement response measurement; (b) Test set-up for shape measurement.

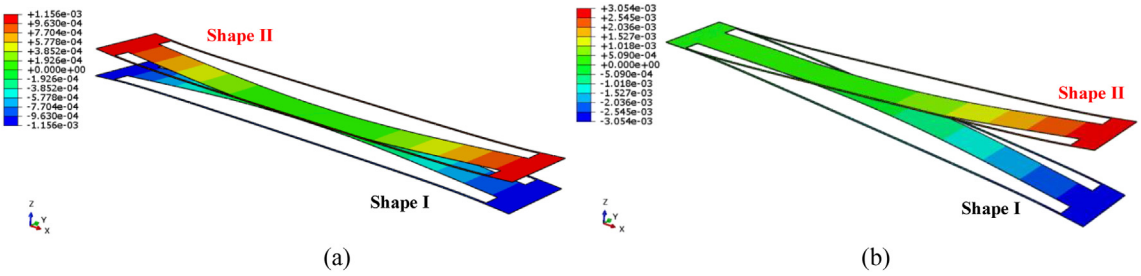

Fig. 7. Out-of-plane displacement contour calculated by FEA: (a) Central fixation; (a) Cantilever boundary.

to trigger the snap-through behavior, and then changing the direction of the displacement makes the prototype snap back in the last step. The load-displacement curves can be extracted from the results given by these two methods, meanwhile, the more information which cannot be captured by experiments is also obtained, such as the deformation process during the snap-through behavior.

5. Results and discussion

5.1. Stable shapes and snap-through behavior

Though this new bistable structure had been fabricated successfully by experiments, the deformation difference between the main beam and supporting beams caused by laser heat is uncertain. In FEA, the deformation difference is caused by the temperature gradient applying to the supporting beams. We attempted to find the assumed equivalent temperature gradient which can meet the results of shape and force-displacement response. Here, the equivalent temperature gradient ΔT applied to the supporting beams is −123 K. To compare with experimental results, the displacement of stable shape *I* is adjusted to zero, so the FEA load-displacement curves also move with the stable shape *I*. The comparison between FEA and experimental results of the shapes and load-displacement responses is illustrated in Fig. 8. The FEA results agree well with experimental results, which approves that this assumed temperature gradient is reasonable and the finite element modeling is reliable.

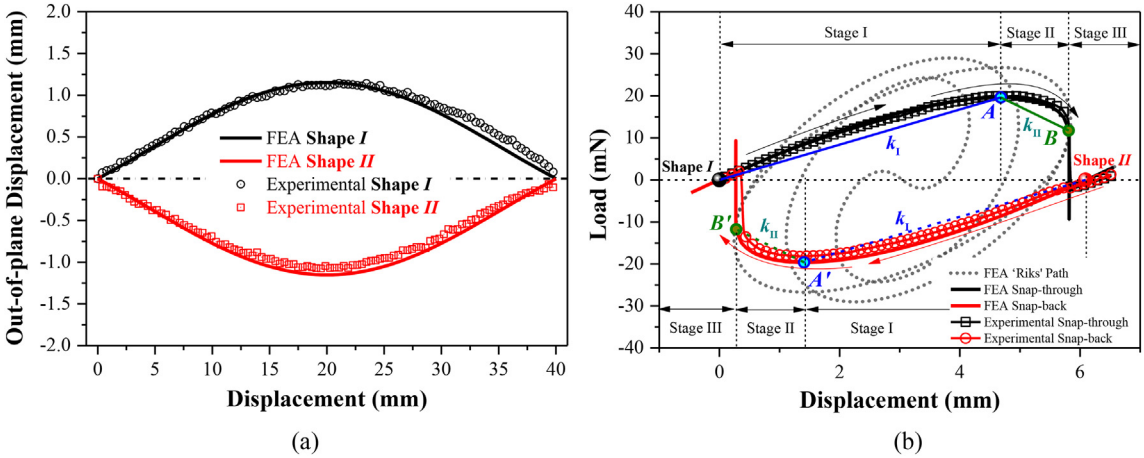

Fig. 8. Comparison between FEA and experimental results: (a) Stable shapes; (b) Load-displacement responses.

The two sine-curved shapes of the main beam in Fig. 8(a) exhibits the bi-stable feature, but the symmetry of the two experimental shapes is not as perfect as the FEA. The experimental shape *I* is in better agreement with FEA, but the curve of the experimental out-of-plane displacement for the shape *II* is slightly lower than that given by FEA. It can be explained that the experimental sample has some imperfections in the thickness direction. The laser-machined incision is a trapezoid, so it is unsymmetrical in geometry condition after fabrication, which is not embodied in FEA.

The load-displacement curves predicted by the 'Stabilize' method have a good agreement with the experimental results, as shown in Fig. 8(b). This bistable structure is triggered in the forward loading direction to snap from the shape *I* to *II* and then snapped back from shape *II* to *I* under opposite-direction load. The load-displacement curve of the snap-through is taken as an example to illustrate its nonlinear characteristics. Starting from the zero (shape *I*), the load increases with displacement slowly meanwhile the stiffness varies from linear character to softening character. After the load reaches the peak value (Point A), namely snapping load, it starts to decrease with negative stiffness, and then the load drops precipitously with a drastic oscillation after passing Point B which is termed as the snap-down point. After dropping to the lowest value, the load increase with the displacement again and arrives at shape *II*, which means this bistable structure completes its snap-through behavior. For the static FEA results, the lowest value does not represent the practical significance, which is removed for comparison with experimental results.

In the backward direction, namely snap-back response, the variation tendency of load with decreasing displacement is similar to that in the forward loading direction. The snapping load corresponding to two loading directions has the same value of 19.63 mN for FEA, but two experimental snapping loads have a difference of 1%. The experimental snapping load in the forward direction is very close to the value given by FEA with an error of 1.7% but the error reaches 7.3% for the snap-back response due to the imperfection of the experimental sample, as illustrated in Table 2. Table 2 also lists the displacements corresponding to the snapping load point and snap-down point in two loading directions. The experimental results and FEA results are very close. From the area bounded by the load-displacement curve and zero-load line, the required energy for snap-through can be calculated, as illustrated in Table 2. Like the snapping load, the error of required energy in the forward loading direction is lower than that in the backward direction. From the above comparison between experimental results and FEA results, it can be concluded that finite element modeling is reliable.

An effective stiffness k_{I} is obtained by connecting the starting point and snapping point on the curve of load-displacement, and the negative effective stiffness k_{II} is obtained similarly, as shown in Fig. 8(b). The value of effective stiffness k_{I} is lower than that of the negative effective stiffness k_{II}. This is slightly different from the traditional bistable curved beam with the two-end constraint, whose value of negative stiffness is lower than that of positive stiffness [9,28–30]. During the snap-back process, k_{I} and k_{II} remain unchanged.

Unlike the single load-displacement response of the pinned-pinned buckling beam with a central actuation regardless of the actuation direction as shown in Fig. 1(b), this bistable structure has two load-displacement curves depending on the actuation direction between two snap-down points (B and B′). Except for this region, the load-displacement response follows the same path regardless of the loading direction. These two load-displacement paths form a 'loop', which is one of the typical hysteresis characteristics. Thus, this cantilever bistable structure has a relatively strong hysteretic response during the transition process between stable states, which makes it have the energy dissipation capacity. The dissipated energy can be obtained from the area of the hysteresis 'loop', which is up to 145 mN·mm. The dissipated energy can be quantified by a general measure of damping called loss factor η [31], which is defined as

$$\eta = E_{\mathrm{d}}/(2\pi W) \tag{7}$$

where E_{d} is the dissipated energy, and W is the required energy of snap-through. From the results in Table 2, the loss factor η is approximately 0.3.

Different from the 'Stabilize' method, the 'Riks' method gives a single load-displacement equilibrium path with the complicated transformation from the shape *I* to *II*, as shown in Fig. 9(a). The direction of the path is also demonstrated, and the positions of two stable shapes are marked. From the comparison between the 'Riks' and 'Stabilize' shown in Fig. 8(b), it is found that the load-displacement curve given by the 'Stabilize' method is a part of the 'Riks' equilibrium path. Two load-displacement curves separate at the snap-down point where the tangent of the 'Riks' path is vertical, and then the 'Riks' equilibrium path turns back, however, the actual load must snap down to the second stable path because there is no equilibrium state near the snap-down point when the displacement is further increased.

To further understand the reason why the load traces the path given by the 'Stabilize' method, the total strain energy with the displacement of this bistable structure is extracted from FEA results, as shown in Fig. 9(b). There are eight critical points are corresponding to positions of the vertical tangent on the 'Riks' load-displacement path, as shown in Fig. 9(a), and these points are also marked on the strain energy curve. It is found that the first and eighth critical points locate at the peak strain energy given by the 'Stabilize' method. The energy barrier ΔE_1 between the stable shape and the first critical point represents the required energy to accomplish the snap-through behavior. The experimental and FEA required energy of snap-through and snap-back is illustrated in Table 2. The remaining critical points in Fig. 9(b) form the other three energy barriers which are much higher than ΔE_1. According to the principle of minimum potential energy, the load will select the path with less energy consumption. Thus, the load-displacement path given by the 'Stabilize' method is in agreement with experimental results.

To reveal the snap-through response further, the deformation process of the main buckling beam represented by the out-of-plane displacement of the longitudinal centerline from the shape *I* to *II* under tip load is extracted from FEA results, as shown in Fig. 10. The curve of load-displacement response predicted by FEA can be divided into three stages, as shown in Fig. 8(b). The first stage covers from the start position to snapping load, the following second stage locates between snapping force and the snap-down point and the last stage represents the phase where the force falls and increases with displacement again. Here, the different types of lines are adapted for different stages, and the critical points, such as stable shapes, snapping load (A), and snap-down point (B), are emphasized in Fig. 10. In the first stage, the deformation of the buckling beam concentrates on the vicinity of the root and extends gradually to the central region. At the end of the first stage corresponding to the snapping load, the buckling beam exhibits a reversed S-shaped configuration. This reversed S-shaped configuration continues to exist in the second stage and the configuration exhibits a more coherent S-shape at the snap-down point, namely the end of the second stage. In the last stage, the displacement on the vicinity of the root rebounds during the falling process of the load until the direction of curvature on the entire beam becomes the same, and the shape of the main beam approaches and passes the shape *II* when the displacement increases further. When the direction of load changes, the deformation process is similar which is also consisted of three stages. From the deformation process, it is found that the transient shape of the main beam corresponding to the snap-down point is similar to the second buckling mode of the pinned-pinned pre-compressed beam with more storing energy than the first buckling mode [3]. Due to this cantilever boundary condition, the transient shape is corresponding to the energy barrier arises at different positions during two actuation processes, which eventually leads to the hysteresis response.

Table 2
Typical mechanical characters of the snap-through behavior.

	Snapping load /mN			Position of snapping load/mm		Position of snap-down point/mm		Required energy/mN·mm		
	Exp.	FEA	Error	Exp.	FEA	Exp.	FEA	Exp.	FEA	Error
Snap-through	19.96	19.63	1.7%	4.60	4.68	5.82	5.81	77.08	77.53	0.6%
Snap-back	18.20	19.63	7.3%	1.38	1.41	0.39	0.28	68.32	77.53	11.9%

5.2. Parametric analysis

According to Eq. (6), the nonlinear snap-through behavior of this proposed bistable structure depending on laser processing parameters and geometrical parameters. Herein, we select four representative parameters to investigate their influence on the bistability.

5.2.1. Temperature gradient

In the finite element modeling, the temperature gradient ΔT applying on the supporting beams represents the level of stress induced by laser heat. During the fabrication process, the laser heat can be adjusted by processing parameters, such as laser power and scan speed. Here, the mechanism of fabrication is not considered and the ideal condition is adopted. Several temperature gradients are performed and the other parameters remain the same. The load-displacement responses of the bistable structure with different temperature gradients during two loading processes are shown in Fig. 11(a).

To make the main beam buckle, it is known from Eq. (6) that the temperature gradient should be high enough to introduce the required stress σ_n. Thus, the bistability will lose if the temperature gradient decreases further to a certain value. When the temperature gradient is significantly higher than the critical value, the bistability is strengthened gradually with ΔT. As expected, the snapping load, the required energy to trigger snap-through, and the displacement corresponding to shape *II* increase with the temperature gradient. Compared to the temperature gradient of -50 K, the snapping load and the required energy to trigger the snap-through increase by 52.2% and 137.6% respectively when ΔT is -100 K. However, the snapping load and the required energy increase by 26.1% and 58.0% when ΔT changes from -100 K to -150 K. Therefore, the snapping load and the required energy of snap-through increase nonlinearly with ΔT, and the growth of snapping load has a slower trend. The area of hysteresis 'loop' also enlarges with the temperature gradient, which means this bistable structure will dissipate more energy when the pre-compression Δ*L* increases. The dissipated energy is almost twice as much as the required energy when the temperature gradient is relatively high. Similarly, the hysteresis becomes weak when ΔT is declining, and the dissipated energy reduces nonlinearly. The loss factor η decreases from 0.32 to 0.26 when ΔT is from -100 K to -20 K. As shown in Fig. 11(a), the load follows the single path regardless of the actuation direction when ΔT is -10 K, which means the hysteresis disappears in this case and loss factor η is zero. Consequently, the temperature gradient is a critical parameter that has a significant influence on the performance of this bistable structure.

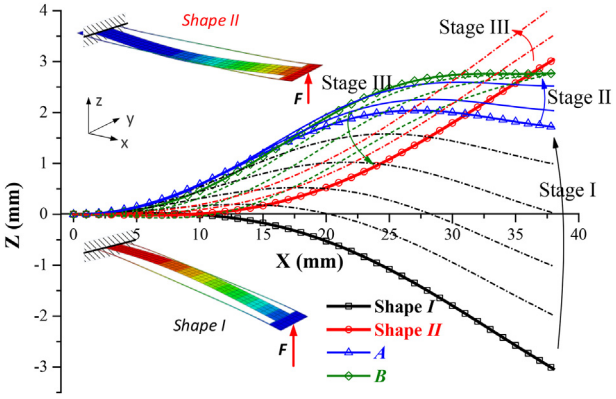

Fig. 10. Cantilever bistable buckling beam deformation process during snap-through behavior.

To illustrate the feasibility of controlling the temperature gradient in the fabrication, laser power representing the carried energy is employed to adjust the bistability. As shown in Fig. 11(b), when the laser power is lowered to 11.1 W, the experimental load-displacement curves have a good agreement with the FEA results with a temperature gradient of -70 K. Compared the snapping load, and the required energy of two bistable structures fabricated by the different laser power, it is concluded that the laser power is one of the critical processing parameters to control the bistability of this laser-machined structure.

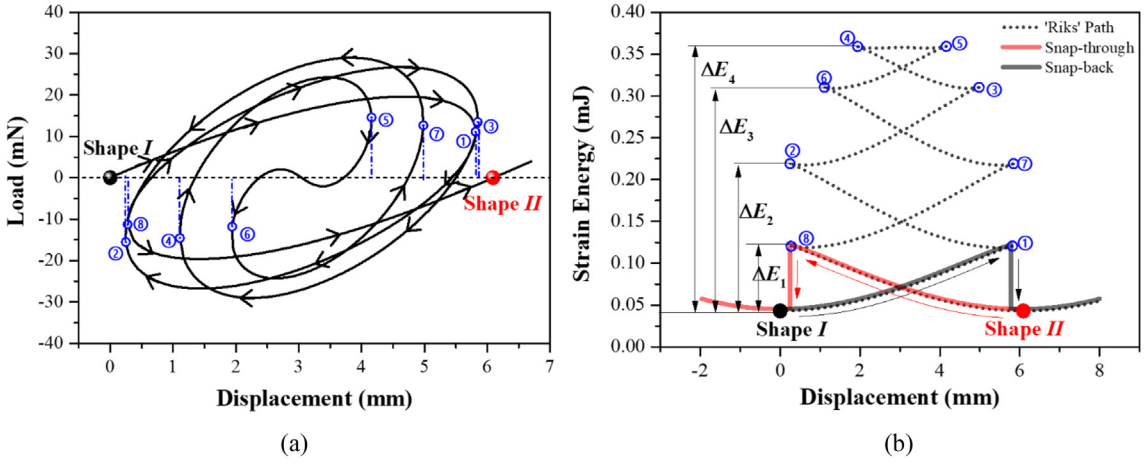

Fig. 9. (a) The load-displacement path given by the 'Riks' method; (b) The total strain energy during the snap-through process.

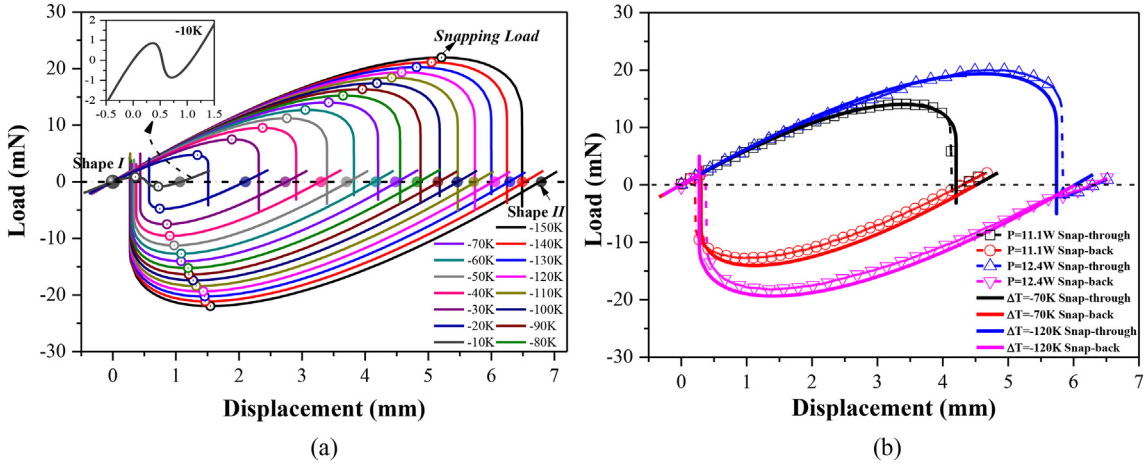

Fig. 11. (a) Load-displacement responses of bistable structure with different temperature gradients predicted by FEA; (b) Comparison between experimental and FEA results.

5.2.2. Width of the main beam

Besides the temperature gradient, the geometries are other important parameters that can be employed to design the performance of this new bistable structure. The width W_1 of the main beam is investigated firstly. The temperature gradient of -123 K and the other geometry parameters remain unchanged, and the width W_1 varies from 2.1 mm to 5.1 mm with an interval of 0.5 mm.

Fig. 12(a) shows the load-displacement responses with different W_1 predicted by FEA. The snapping load and required energy to trigger shape transition increase with the width of the main beam, but the displacement corresponding to the shape *II* is almost unchanged. Due to the certain temperature gradient, the pre-compression ΔL applying the main beam is almost constant, so the stable shape represented by Eqs. (1) is the same for different W_1, and the snap-down point also locates the neighboring area. The rigidity *EI* of the main beam increases with its width, so the load-displacement curve for the wider beam has a higher stiffness k_I on the way of reaching the snapping load. The value of negative stiffness k_{II} between snapping load and snap-down point also increases with W_1. When the width is 5.1 mm, the required energy for snap-through behavior is 2.1 times more than that of 2.1 mm and the snapping load has a similar relationship like this. Thus, the snapping load and required energy increase with W_1 in the same proportion. The dissipated energy of hysteresis related to the required energy also has a similar tendency, but the loss factor η has not changed much.

To verify the impact of W_1, a prototype with a width of 4.6 mm was fabricated through the same laser processing parameters as previously. Its experimental load-displacement responses of snap-through behavior are compared with FEA results, as illustrated in Fig. 12(b). The experimental results agree with the results predicted by FEA. The stiffness k_I represented by load slope and the snapping load of the prototype with the width W_1 of 4.6 mm is higher than that when W_1 is 3.6 mm. Due to the imperfection, the experimental snapping load in two loading direction has a difference of 5.3%. However, these results have demonstrated that the bistability will be strengthened by increasing the width of the main beam.

5.2.3. Width of the supporting beam

The second geometry parameter is the width W_2 of the supporting beam. The temperature gradient of -123 K is supposed to apply on the supporting beams and the load-displacement responses with different width W_2 predicted by FEA are shown in Fig. 13(a). It is found that the bistability is reinforced when the width of the supporting beam becomes wider, which is reified by increasing snapping load, slop of load, and required energy with W_2. The other point noted is that the displacement corresponding to the snap-down point is higher than that of shape *II* when W_2 increases to 0.8 mm. However, in the basic concept of this bistable structure, the pre-compression ΔL to make the main beam buckle is the difference of deformation between the main beam and supporting beam induced by the laser fabrication. When the supporting

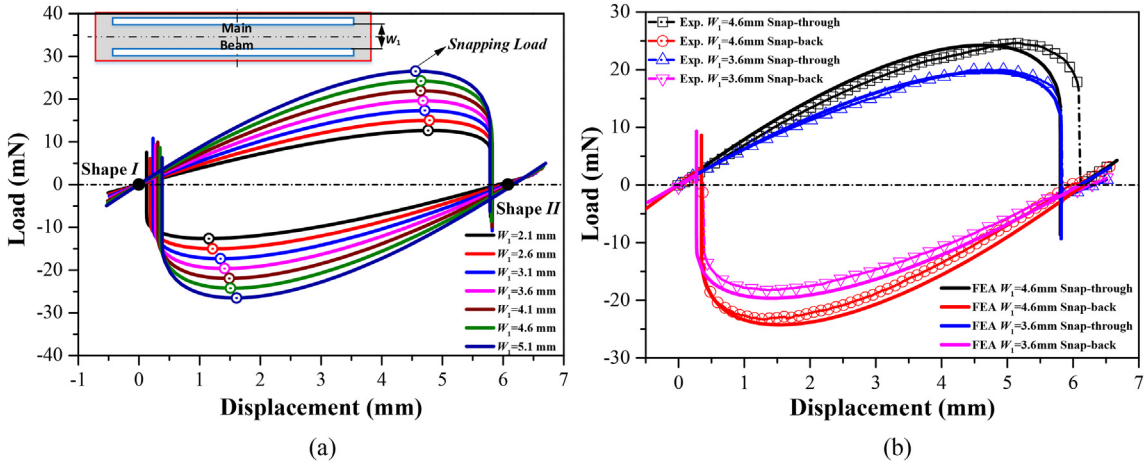

Fig. 12. (a) Load-displacement responses of the bistable structure with different width W_1 of the main beam predicted by FEA; (b) Comparison between experimental and FEA results.

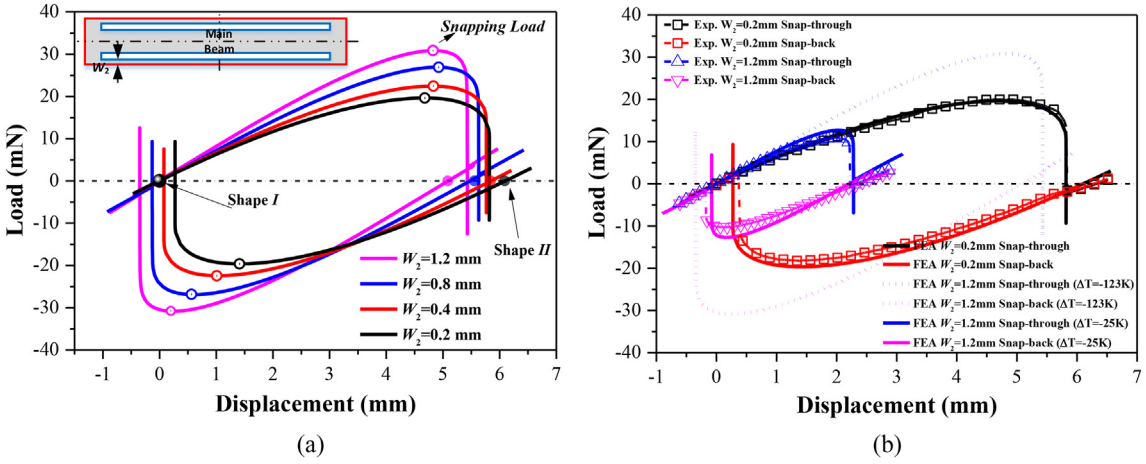

Fig. 13. (a) Load-displacement responses of the bistable structure with different width W_2 of the supporting beam predicted by FEA; (b) Comparison between experimental and FEA results.

beam becomes wider, the distance between two heat-affected zones containing residual stress increases, and the influence of the residual stress on the supporting beam becomes weaker. Thus, the difference of deformation between the main beam and supporting beam, namely pre-compression ΔL, decreases, and the bistability is weakened.

To understand the influence of W_2 on the bistability, a sample with W_2 of 1.2 mm was fabricated by previous laser processing parameters and its load-displacement responses were tested, as illustrated in Fig. 13(b). The experimental results are vastly different from the FEA results with the temperature gradient of -123 K. A new temperature gradient of -25 K is found to match the experimental results. In the finite element model, the pre-compression ΔL induced by laser is represented by the temperature gradient, so this demonstrates that the pre-compression ΔL is decreasing with the increase of W_2 even the processing parameters remain unchanged. These results validate the proposed new concept which utilizes the difference of thermal deformation between the main beam and supporting beams to pre-compress the main beam to buckle. Therefore, the width of the supporting beam is an important geometry parameter to realize this bistable structure.

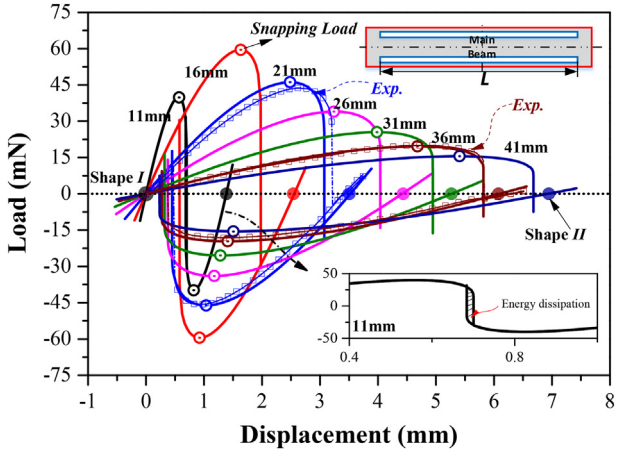

Fig. 14. Load-displacement responses of the bistable structure with different length L of the beam.

5.2.4. Length of beam

Fig. 14 demonstrates that the load-displacement responses of the bistable structure with different lengths of the beam. The length of two ends maintains as a constant and the length L of the beam decreases from 41 mm to 11 mm with an interval of 5 mm. The temperature gradient ΔT is considered as a constant of -123 K because of the unchangeable laser processing parameters.

It is observed that the displacement corresponding to shape *II* and the stiffness k_1 increase with L, but the snapping load increase and then decline with L. The required energy of snap-through also increases firstly and then decreases with L, but the length corresponding to the highest required energy is 21 mm but not is 16 mm with the highest snapping load. Likewise, the hysteresis response is disappearing when the length is declining. When the length is 11 mm, the hysteresis 'loop' becomes very small and the dissipated energy is only 0.08 mN·mm, as shown in Fig. 14, and the loss factor η is only 0.0007. A new prototype with a length of 21 mm was fabricated and its load-displacement responses have a good agreement with the FEA results,

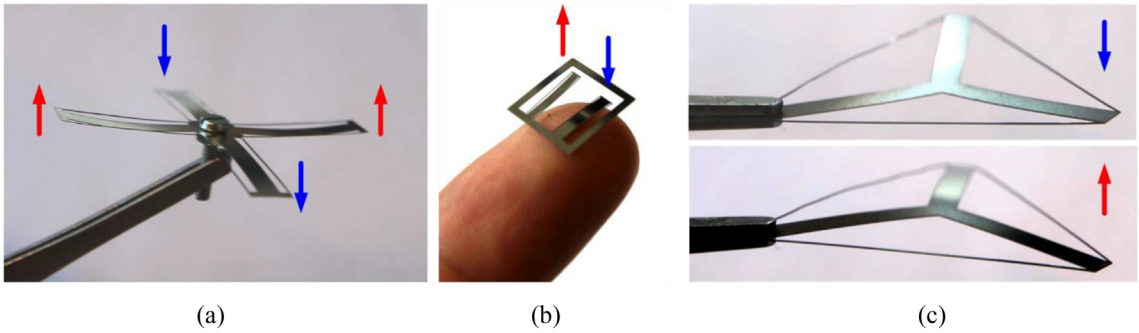

Fig. 15. (a) Cross-shaped multistable structure; (b) Bistable structure with small size; (c) Triangle bistable structure.

which validated the effect of length on the performance of this bistable structure. From Eq. (6) and Fig. 4, the required stress σ_n increases when the beam becomes shorter, so the bistability will gradually disappear with decreasing L in the case of the unchanged temperature gradient.

The above results about geometry parameters illustrate that the performance of bi-stability can be maintained despite the whole sample becomes smaller than before. Therefore, the size of this proposed bistable structure has the potential to decrease further.

6. Other innovative designs and potential applications

The above results have demonstrated that the concept of taking laser machining as both of the fabrication method and the pre-stressing method to design and manufacture the bistable compliant structure is feasible. However, this concept can be extended for further innovative designs. As shown in Fig. 15, we have verified the other three cases successfully. Four bistable cantilevers sharing one end compose a cross-shaped multistable structure, and one of its stable shapes is shown in Fig. 15(a), where the direction of the arrow represents the bending direction. We also reduced the size of the proposed bistable structure further and fabricated one sample with the fingertip size shown in Fig. 15 (b). Another case is considered that the supporting beams are not parallel to the buckled main beam anymore and there is an angle between supporting beams and the main beam. One triangle bistable structure is designed and fabricated shown in Fig. 15(c).

Concerning the characteristics of the proposed bistable structure, we will exploit its potential applications in the future. One potential application is that the bistable structure acting as a host structure combines the piezoelectric materials to form the energy harvester. Due to the bistability, the harvester has nonlinear dynamic features, which make it realize the broadband vibrational energy harvesting. Compared to the bistable energy harvester with two-end constraints, the cantilever configuration makes it have a much lower natural frequency when the size is small. Additionally, the bending shape of the main beam is conducive to increase the effective area of piezoelectric material. Through the configuration shown in Fig. 15(a), the array of bistable energy harvesters is also feasible. Another potential application is damper because of its strong dissipated energy feature. Though the dissipated energy is not high using one sample, a lattice structure assembly an array of samples can be implemented to absorb more energy.

7. Conclusions

In the present study, a new design, and a manufacturing method for the compliant bistable structure is proposed by taking the pulsed laser as both of the fabrication method and the pre-stressing method. One typical case consisted of one wide main beam, and two narrow supporting beams is designed and fabricated successfully. Due to the difference in distance between two heat-affected zones, the deformation difference between the main beam and supporting beams arises after a single machining step with proper laser processing parameters. Benefited from this deformation difference, the main beam will be pre-compressed and exhibit bistability due to the constraints by supporting beams.

Due to the use of a bistable beam and the internal integrated constraint conditions, this bistable structure behaves like a cantilever and can be connected to other components easily. Under this cantilever boundary, two paths depended on the loading direction exhibit on the load-displacement curves between two snap-down points, so this bistable structure has a strong hysteresis feature and the dissipated energy is almost twice of the required energy to trigger the snap-through. Moreover, its tip experiences an impressive 'stroke' during the shape transition.

The effects of changing the manufacturing and geometric parameters of this compliant bistable structure are investigated both experimentally and numerically to further study its bistability mechanism. Its bistability becomes weaker until it disappears with the decreasing of laser power in terms of the temperature gradient. In the case of unchanged laser processing parameters, the snap-through properties including snapping force and required energy are also affected by geometric parameters and the width of the supporting beam is the key parameter to realize this bistable structure. The results of the parametric analysis illustrate that the proposed method has the potentials of shorter pre-compressed beam lengths and smaller device areas.

Another three cases with multistable features or smaller size are validated experimentally to illustrate that the proposed method is feasible and promotional. This family of the bistable structure obtained by the proposed method has the potential applications of damper or energy harvester due to the feature of dissipated energy.

Declaration of Competing Interest

The authors declared that they have no conflicts of interest to this work.

Acknowledgment

The authors thank Jos van Driel for assisting in the experimental measurement in this work. This work is supported by the National Natural Science Foundation of China [grant No. 11772107], China Scholarship Council, and STW on the Veni project [No. 14379].

We declare that we do not have any commercial or associative interest that represents a conflict of interest in connection with the work submitted.

References

[1] N. Hu, R. Burgueño, Buckling-induced smart applications: recent advances and trends, Smart Mater. Struct. 24 (2015), 063001.
[2] X. Liu, F. Lamarque, E. Doré, P. Pouille, Multistable wireless micro-actuator based on antagonistic pre-shaped double beams, Smart Mater. Struct. 24 (2015), 075028.
[3] J. Qiu, J.H. Lang, A.H. Slocum, A curved-beam bistable mechanism, J. Microelectromech. Syst. 13 (2004) 137–146.
[4] G. Hao, J. Mullins, On the Comprehensive Static Characteristic Analysis of a Translational Bistable Mechanism, 230, 2016 3803–3817.
[5] C.S. Ha, R.S. Lakes, M.E. Plesha, Design, fabrication, and analysis of lattice exhibiting energy absorption via snap-through behavior, Mater. Des. 141 (2018) 426–437.
[6] C. Valencia, D. Restrepo, N.D. Mankame, P.D. Zavattieri, J. Gomez, Computational characterization of the wave propagation behavior of multi-stable periodic cellular materials, Extreme Mech. Lett. 33 (2019) 100565.
[7] X. Tan, B. Wang, S. Chen, S. Zhu, Y. Sun, A novel cylindrical negative stiffness structure for shock isolation, Compos. Struct. 214 (2019) 397–405.
[8] B. Ando, S. Baglio, A.R. Bulsara, V. Marletta, V. Ferrari, M. Ferrari, A low-cost snap-through-buckling inkjet-printed device for vibrational energy harvesting, Sensors J. IEEE. 15 (2015) 3209–3220.
[9] B. Camescasse, A. Fernandes, J. Pouget, Bistable buckled beam and force actuation: experimental validations, Int. J. Solids Struct. 51 (2014) 1750–1757.
[10] B. Camescasse, A. Fernandes, J. Pouget, Bistable buckled beam: Elastica modeling and analysis of static actuation, Int. J. Solids Struct. 50 (2013) 2881–2893.
[11] J. Cleary, H.-J. Su, Modeling and experimental validation of actuating a bistable buckled beam via moment input, J. Appl. Mech. 82 (2015).
[12] M. Nistor, R. Wiebe, I. Stanciulescu, Relationship between Euler buckling and unstable equilibria of buckled beams, Int. J. Non-Linear Mech. 95 (2017) 151–161.
[13] R. Gao, M. Li, Q. Wang, J. Zhao, S. Liu, A novel design method of bistable structures with required snap-through properties, Sensors Actuators A Phys. 272 (2018) 295–300.
[14] Y. Zhang, Q. Wang, M. Tichem, F. van Keulen, Design and characterization of multistable mechanical metastructures with level and tilted stable configurations, Extreme Mech. Lett. 100593 (2019).
[15] I.Z. Pane, T. Asano, Investigation on bistability and fabrication of bistable prestressed curved beam, Jpn. J. Appl. Phys. 47 (2008) 5291–5296.
[16] I.Z. Pane, T. Asano, Analysis and fabrication of ampere-force actuated bistable curved beam, Jpn. J. Appl. Phys. 48 (2009) (06FK8).
[17] Q. McCulloch, J.G. Gigax, P. Hosemann, Femtosecond laser ablation for mesoscale specimen evaluation, JOM. 72 (2020) 1694–1702.
[18] L. Yang, Y. Ding, B. Cheng, A. Mohammed, Y. Wang, Numerical simulation and experimental research on reduction of taper and HAZ during laser drilling using moving focal point, Int. J. Adv. Manuf. Technol. 91 (2017) 1171–1180.

[19] C. Ni, L. Zhu, Z. Zheng, J. Zhang, Y. Yang, R. Hong, et al., Effects of machining surface and laser beam scanning strategy on machinability of selective laser melted Ti6Al4V alloy in milling, Mater. Des. 194 (2020) 108880.
[20] D. Almonti, G. Baiocco, V. Tagliaferri, N. Ucciardello, Design and Mechanical Characterization of Voronoi Structures Manufactured by Indirect Additive Manufacturing, 13, 2020 1085.
[21] S. Liu, Y.C. Shin, Additive manufacturing of Ti6Al4V alloy: a review, Mater. Des. 164 (2019) 107552.
[22] H. Al-Ethari, A. Hobi, O. Ali, Optimization of manufacturing parameters affecting on characterization of porous sintered tin-bronze alloy, Int. J. Eng. Technol. 8 (2019) 299–307.
[23] M.Z. Mohd Zin, E.H. Felix, Y. Wahab, M.N. Bakar, Process development and characterization towards microstructural realization using laser micromachining for MEMS, SN Appl. Sci. 2 (2020) 912.
[24] N. Samotaev, K. Oblov, M. Etrekova, D. Veselov, A. Gorshkova, Parameter studies of ceramic MEMS microhotplates fabricated by laser micromilling technology, Mater. Sci. Forum 977 (2020) 238–243.
[25] B.S. Yilbas, A.F.M. Arif, Laser cutting of steel and thermal stress development, Opt. Laser Technol. 43 (2011) 830–837.
[26] M. Ansari, M.A. Karami, Energy harvesting from controlled buckling of piezoelectric beams, Smart Mater. Struct. 24 (2015) 115005.
[27] A. Arif, B.S. Yilbas, Thermal stress developed during the laser cutting process: consideration of different materials, Int. J. Adv. Manuf. Technol. 37 (2008) 698–704.
[28] P. Cazottes, A. Fernandes, J. Pouget, M. Hafez, Bistable buckled beam: modeling of actuating force and experimental validations, J. Mech. Des. 131 (2009) 101001–101010.
[29] J.-S. Chen, S.-Y. Hung, Snapping of an elastica under various loading mechanisms, Eur. J. Mech. A/Solids. 30 (2011) 525–531.
[30] W. Yan, Y. Yu, A. Mehta, Analytical modeling for rapid design of bistable buckled beams, Theor. Appl. Mech. Lett. 9 (2019) 264–272.
[31] M. Alturki, R. Burgueño, Multistable cosine-curved dome system for elastic energy dissipation, J. Appl. Mech. 86 (2019).